JOURNAL OF THEORETICAL
AND APPLIED MECHANICS
https://doi.org/10.15632/jtam-pl/201245
ONLINE FIRST

VIBRATION ANALYSIS AND CONTROL OF 2SPS+SR SUSPENSION SEAT FOR IMPROVING VEHICLE RIDE COMFORT

Bijuan YAN*, Haiqing ZHANG, Yihang GENG, Wenjun ZHANG

Taiyuan University of Science and Technology, 030024, Taiyuan, Shanxi, China
*corresponding author, *tyustybj@tyust.edu.cn*

In order to minimize three-dimensional vibrations and improve the ride comfort of a construction vehicle, the 2-spherical-prismatic-spherical+spherical-revolute (2SPS+SR) parallel suspension seat is examined. The dynamic differential equations of the seven degree-of-freedom (DOF) vehicle and the seat model are derived. Under E-, F-, and G-level roads (classified based on standard or index, e.g., ISO 8608, for road roughness), the dynamic responses of the 2SPS+SR seat are analyzed. The simulation results indicate that the seat comfort performance using fuzzy-PID control is enhanced by 40.91 %, 19.84 %, and 36.40 %, which are compared with PID under E-, F-, and G-level roads, respectively.

Keywords: construction vehicle; 2SPS+SR seat suspension; ride comfort; fuzzy-PID.

1. Introduction

Construction vehicles play an important role for assisting employees and increasing their work efficiency in modern economic development. However, they often travel or work on off-roads, the working environments are very poor. Mechanical vibrations in different directions from the source of vibration are transmitted to the drivers through the tires, vehicle suspensions, suspension cab and seat (Yan *et al.*, 2022). The operators react to the unwanted vibrations due to psychological and physiological reasons. The relevant studies in (Desai *et al.*, 2021) show that humans respond differently to vibrations of different frequencies. At the same time, the vibration frequency of vehicles is also located between 0 Hz–20 Hz. Therefore, these vibrations cause adverse health effects for drivers to a certain extent and reduce the service life of vehicle components. So, reducing the vibrations of construction vehicles especially in the low frequency range has become a research hotspot in recent years.

Nowadays, the seat suspension systems are widely used to attenuate whole-body vibration exposure on drivers. For example, Deng *et al.* (2022) investigated a seat suspension installed with rotary magnetorheological dampers to avoid end-stop impact. The negative-stiffness-structure seat suspensions are designed to further ameliorate the vehicle ride quality for different vibration conditions (Ni *et al.*, 2023). Tan *et al.* (2021) used an air suspension system to improve the ride comfort of buses. However, considering that the seated human body is sensitive to the pitch vibration of vehicles, the parallel mechanisms have been applied to vehicle seats to achieve multi-dimensional vibration reduction from the cab to the driver (Sun *et al.*, 2023). For example, Zhang *et al.* (2015) proposed a 3-revolute-prismatic-cylindrical (3-RPC) parallel mechanism combined with energy dissipation components to achieve multi-dimensional vibration reduction. Wu *et al.* (2011) proposed a three-translation parallel mechanism which can make the human body have a better ride comfort.

On the other hand, the seat suspension systems could be classified into three types including passive, semi-active and active suspensions from the view of control modes. Early researches mainly focused on the passive seat suspension, but its damping performance is unsatisfactory

once the vehicle working conditions change. Therefore, in order to solve the above questions, the semi-active and active control become more and more popular. For example, Abdul Zahra and Abdalla (2020) use the combination of fuzzy super twisting sliding mode concept (FSTSMC) and PID controller to improve the comfort of the driver under random road. Khan *et al.* (2016) established an active controller of vehicle suspension systems. With the development of magnetorheological (MR), semi-active suspensions using these smart materials are used and studied by many researchers. For example, Zhang and Zhao (2017) proposed a semi-active car seat suspension with MR damper, and compared three control methods of fuzzy sliding mode controller with expansion factor (FSMCEF), PID, and SMC. Jain *et al.* (2020) proposed a semi-active seat suspension based on MR dampers. Maciejewski *et al.* (2020) analyzed an active vibration damping system with a seated human body. And a new control strategy for permanent magnet synchronous motors is proposed. Based on the mathematical model of mass-spring-damper (MSD) system, Maciejewski *et al.* (2020) proposed the horizontal seat suspension system using sliding mode control (SMC) strategy. It can be seen from the above-mentioned documents that most on current research seat suspensions are based on road vehicles such as automobiles, there are few studies about "off-road" construction vehicles.

Based on the above researches, this paper studies the vibration-reducing performance of the kind of 2SPS+SR parallel suspension seat. In order to verify its three-directional movements, the single-open-chain theory is used to obtain the position and orientation characteristics (POC) set of the seat. The motion differential equations of the seven-DOF vehicle and three-DOF 2SPS+SR suspension seat is established. A fuzzy PID controller that applies the seat acceleration variables as feedback signals is proposed, which can control the vertical, fore-aft and lateral vibration of the vehicle. And the vibration reduction performance of the seat suspension and the ride comfort of the drivers under different control and different roads are compared.

2. Physical model of 2SPS+SR seat suspension

2.1. Structure of 2SPS+SR seat suspension

As is shown in Fig. 1, the new 2SPS+SR parallel seat suspension is equipped with three evenly distributed limbs, in which two limbs are composed of moving and spherical pairs

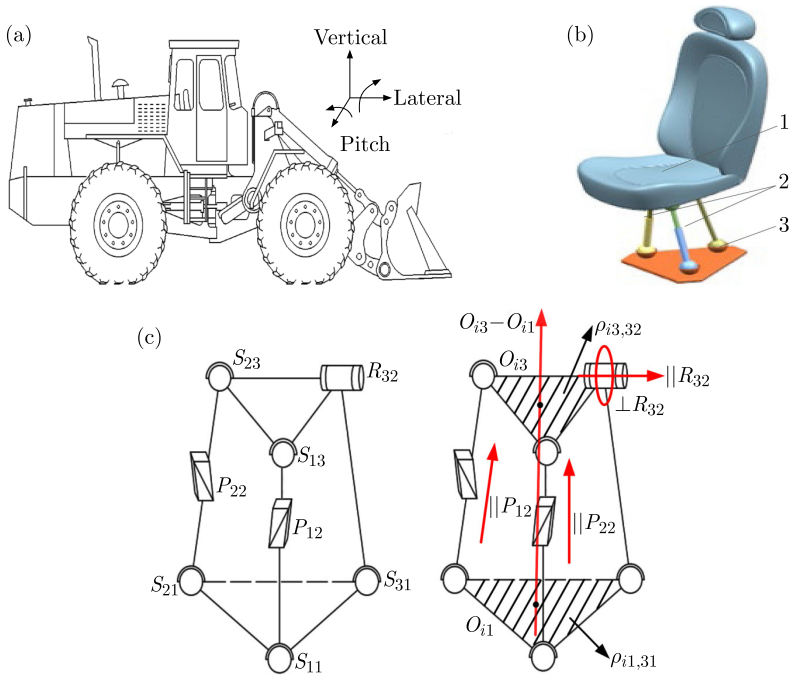

Fig. 1. 2SPS+SR seat suspension of construction vehicle: (a) construction vehicle; (b) seat model (1 – seat, 2 – moving pair, 3 – rotary pair); (c) 2SPS+SR parallel structure.

$\{-S_{i1}-P_{i2}-S_{i3}-\}$ $(i=1,2)$ and the other limb consists of spherical and rotary pairs $\{-S_{31}-R_{32}-\}$. Here, S stands for spherical pair, P is moving pair, and R is rotary pair.

2.2. Vertical-pitch-lateral movement verification

Based on the single-open-chain theory (Yang, 2012), POC sets of the limbs $\{-S_{i1}-P_{i2}-S_{i3}-\}$ $(i=1,2)$ are is described as follows:

$$\begin{aligned} M_{bi} &= \begin{bmatrix} t^1(\parallel P_{i2}) \\ r^0 \end{bmatrix} \cup \begin{bmatrix} t^2(\perp\rho_{i3,32}) \\ r^3(O_{i3}) \end{bmatrix} \cup \begin{bmatrix} t^2(\perp\rho_{i1,3i}) \\ r^3(O_{i1}) \end{bmatrix} \\ &= \begin{bmatrix} t^1(\parallel P_{i2}) \cup \left\{t^2(\perp\rho_{i3,32}) \cup \left\{t^2(\perp\rho_{i1,31}\right\}\right\} \\ r^3(O_{i3-i1}) \end{bmatrix}, \qquad i=1,2 \end{aligned} \tag{2.1}$$

where $t^1(\parallel P_{i2})$ represents a movement which is parallel to the P_{i2} axis, $t^2(\perp\rho_{i3,32})$ denotes two movements which are perpendicular to the $\rho_{i3,32}$ direction, $t^2(\perp\rho_{i1,3i})$ denotes two movements of the chain end which are perpendicular to the vector $\rho_{i1,3i}$, and $r^3(O_{i3}–O_{i1})$ shows that there are three rotations which are perpendicular to the axis $O_{i3}–O_{i1}$.

The POC set of the $\{-S_{31}-R_{32}-\}$ chain are defined as follow:

$$M_{b1} = \begin{bmatrix} t^1(\perp R_{32}) \\ r^1(\parallel R_{32}) \end{bmatrix} \cup \begin{bmatrix} t^0 \\ r^2(O_{31}) \end{bmatrix} = \begin{bmatrix} t^1(\perp R_{32}) \\ r^2(O_{31}) \end{bmatrix}, \tag{2.2}$$

where $t^1(\perp R_{32})$ denotes one movement of the chain end which is vertical to the axis R_{32}, $r^2(O_{31})$ is chosen for two rotations which are vertical to the axis O_{31}.

Therefore, the POC set of the whole 2SPS+SR parallel seat suspension is obtained:

$$\begin{aligned} M_{Pa} &= \begin{bmatrix} [t^1(\perp R_{32}) \cap [t^1(\perp P_{12}) \cup t^2(\perp\rho_{13,32})] \cap [t^1(\perp P_{22}) \cup t^2(\perp\rho_{23,32})] \\ [r^2(O_{31})] \cap [r^3(O_{13-11})] \cap [r^3(O_{23}-O_{21})] \end{bmatrix} \\ &= \begin{bmatrix} [t^1(\perp R_{32})] \cap [t^1(\perp P_{12})] \cup [t^2(\perp\rho_{13,32})] \cap [t^1(\perp P_{22})] \cup [t^2(\perp\rho_{23,32})] \\ [r^1(\parallel (O_{13}-O_{11}))] \cup [r^1(\parallel (O_{23-21}))] \cup [r^1(\parallel (O_{11},O_{21},O_{31}))] \end{bmatrix}. \end{aligned} \tag{2.3}$$

As can be seen from Eq. (2.3), the POC set of the new type 2SPS+SR parallel seat suspension has three independent elements, and it could realize the desired three-dimensional vertical-pitch-lateral movements. As a results, the seat suspension structure is feasible and reasonable. Figure 2 shows the 2SPS+SR parallel seat suspension.

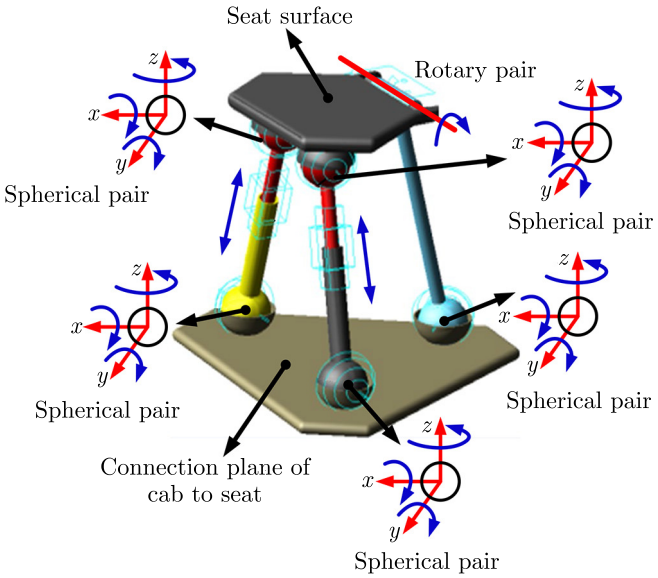

Fig. 2. 2SPS+SR parallel seat suspension.

3. Mathematical model of seat suspension

3.1. Seven degree-of-freedom vehicle model

In this paper, the seven DOF model (depicted in Fig. 3) is used to evaluate the ride comfort of the proposed 2SPS+SR parallel seat suspension. In Fig. 3, m_s and m_{wi} $(i = 1, 2, 3, 4)$ are the mass for the vehicle body and the i-th mass of wheel axles, m_s is the unsprung mass, m_{wi} $(i = 1, 2, 3, 4)$ is the i-th sprung mass, respectively; c_i and k_i $(i = 1, 2, 3, 4)$ denote damping and stiffness coefficients for the vehicle suspensions; c_{ti} and k_{ti} $(i = 1, 2, 3, 4)$ represent the damping and stiffness of tires, a and b are the distances of unsprung masses to the center of gravity of the axles, f and d are the distances between the center of the vehicle body and the front or rear axles; z_{si} and z_{ui} $(i = 1, 2, 3, 4)$ are the vertical displacements of the four support points on vehicle body and suspension systems (base), z_{gi} is the i-th road excitations; z_s, θ, ϕ are the vibration outputs of the vehicle body.

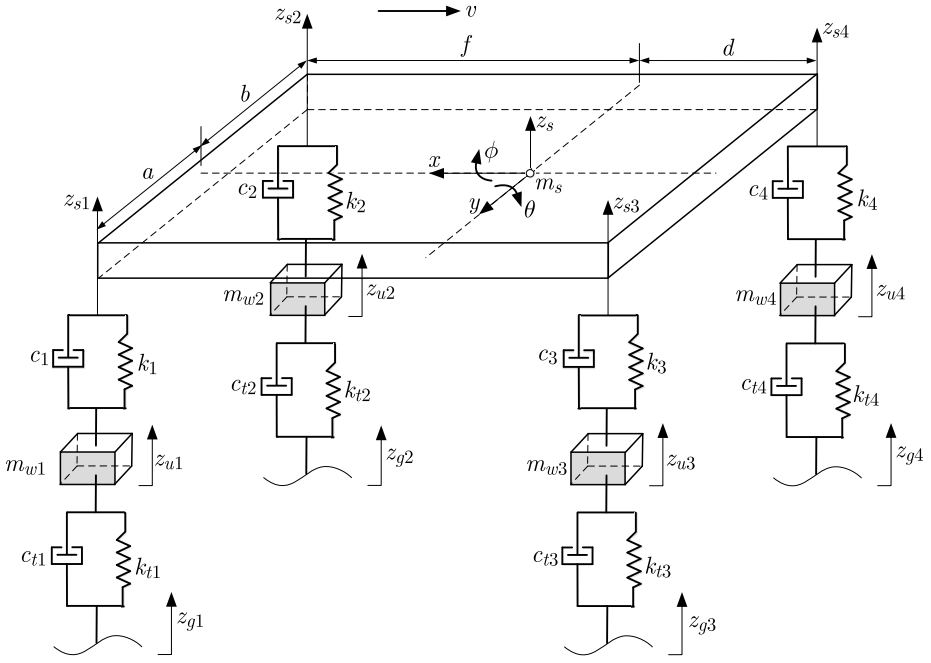

Fig. 3. Seven-DOF vehicle model.

The vertical displacement of the four support points on the vehicle body z_{si} $(i = 1, 2, 3, 4)$ could be obtained by:

$$\begin{aligned} z_{s1} &= z_s + f\theta + a\phi, \qquad & z_{s2} &= z_s + f\theta - b\phi, \\ z_{s3} &= z_s - d\theta + a\phi, \qquad & z_{s4} &= z_s - d\theta - b\phi. \end{aligned} \tag{3.1}$$

The mathematical model that describes a vertical motion of the vehicle body can be written as follows:

$$\begin{aligned} m_s\ddot{z}_s + k_1(z_{s1} - z_{u1}) + c_1(\dot{z}_{s1} - \dot{z}_{u1}) + k_2(z_{s2} - z_{u2}) + c_2(\dot{z}_{s2} - \dot{z}_{u2}) \\ + k_3(z_{s3} - z_{u3}) + c_3(\dot{z}_{s3} - \dot{z}_{u3}) + k_4(z_{s4} - z_{u4}) + c_4(\dot{z}_{s4} - \dot{z}_{u4}) = 0. \end{aligned} \tag{3.2}$$

And the differential equation of the vehicle unit in the pitch direction is established:

$$\begin{aligned} I_{yy}\ddot{\theta} - k_1(z_{s1} - z_{u1}) \cdot f - c_1(\dot{z}_{s1} - \dot{z}_{u1}) \cdot f - k_2(z_{s2} - z_{u2}) \cdot f - c_2(\dot{z}_{s2} - \dot{z}_{u2}) \cdot f \\ + k_3(z_{s3} - z_{u3}) \cdot d + c_3(\dot{z}_{s3} - \dot{z}_{u3}) \cdot d + k_4(z_{s4} - z_{u4}) \cdot d + c_4(\dot{z}_{s4} - \dot{z}_{u4}) \cdot d = 0. \end{aligned} \tag{3.3}$$

The roll movement differential equation is expressed by using the following relation:

$$I_{xx}\ddot{\phi} + k_1(z_{s1} - z_{u1}) \cdot a + c_1(\dot{z}_{s1} - \dot{z}_{u1}) \cdot a - k_2(z_{s2} - z_{u2}) \cdot b - c_2(\dot{z}_{s2} - \dot{z}_{u2}) \cdot b + k_3(z_{s3} - z_{u3}) \cdot a + c_3(\dot{z}_{s3} - \dot{z}_{u3}) \cdot a - k_4(z_{s4} - z_{u4}) \cdot b - c_4(\dot{z}_{s4} - \dot{z}_{u4}) \cdot b = 0. \quad (3.4)$$

In addition, the vertical movement differential equations of four unsprung masses of the vehicle body are obtained as follows:

$$\begin{aligned} &m_{w1}\ddot{z}_1 + k_1(z_{u1} - z_{s1}) + c_1(\dot{z}_{u1} - \dot{z}_{s1}) + k_{t1}(z_{u1} - z_{g1}) + c_{t1}(\dot{z}_{u1} - \dot{z}_{g1}) = 0, \\ &m_{w2}\ddot{z}_2 + k_2(z_{u2} - z_{s2}) + c_2(\dot{z}_{u2} - \dot{z}_{s2}) + k_{t2}(z_{u2} - z_{g2}) + c_{t2}(\dot{z}_{u2} - \dot{z}_{g2}) = 0, \\ &m_{w3}\ddot{z}_3 + k_3(z_{u3} - z_{s3}) + c_3(\dot{z}_{u3} - \dot{z}_{s3}) + k_{t3}(z_{u3} - z_{g3}) + c_{t3}(\dot{z}_{u3} - \dot{z}_{g3}) = 0, \\ &m_{w4}\ddot{z}_4 + k_4(z_{u4} - z_{s4}) + c_4(\dot{z}_{u4} - \dot{z}_{s4}) + k_{t4}(z_{u4} - z_{g4}) + c_{t4}(\dot{z}_{u4} - \dot{z}_{g4}) = 0. \end{aligned} \quad (3.5)$$

Substituting Eq. (3.1) to Eqs. (3.2)–(3.5), the seven DOF vehicle model is obtained as follows:

$$m_s\ddot{z}_s + (c_1 + c_2 + c_3 + c_4)\dot{z}_s + (c_1f + c_2f - c_3d - c_4d)\dot{\theta} + (c_1a - c_2b + c_3a - c_4b)\dot{\phi} - c_1\dot{z}_{u1} - c_2\dot{z}_{u2} - c_3\dot{z}_{u3} - c_4\dot{z}_{u4} + (k_1 + k_2 + k_3 + k_4)z_s + (k_1f + k_2f - k_3d - k_4d)\theta + (k_1a - k_2b + k_3a - k_4b)\phi - k_1z_{u1} - k_2z_{u2} - k_3z_{u3} - k_4z_{u4} = 0, \quad (3.6)$$

$$I_{yy}\ddot{\theta} + (-c_1f - c_2f + c_3d + c_4d)\dot{z}_s + (-c_1f^2 + c_2f^2 - c_3d^2 - c_4d^2)\dot{\theta} + (-c_1af + c_2bf + c_3ad - c_4bd)\dot{\phi} + fc_1\dot{z}_{u1} + fc_2\dot{z}_{u2} - c_3d\dot{z}_{u3} - c_4d\dot{z}_{u4} + (-k_1f - k_2f + k_3d + k_4d)z_s + (-k_1f^2 - k_2f^2 - k_3d^2 - k_4d^2)\theta + (-k_1fa + k_2bf - k_3ad - k_4bd)\phi + fk_1z_{u1} + fk_2z_{u2} - dk_3z_{u3} - dk_4z_{u4} = 0, \quad (3.7)$$

$$I_{xx}\ddot{\phi} + (c_1a - c_2b + c_3a - c_4b)\dot{z}_s + (c_1fa - c_2fb - c_3da + c_4db)\dot{\theta} + (c_1a^2 + c_2b^2 + c_3a^2 + c_4b^2)\dot{\phi} - c_1a\dot{z}_{u1} + c_2b\dot{z}_{u2} - c_3a\dot{z}_{u3} + c_4b\dot{z}_{u4} + (k_1a - k_2b + k_3a - k_4b)z_s + (k_1fa - k_2fb - k_3da + k_4db)\theta + (k_1a^2 + k_2b^2 + k_3a^2 + k_4b^2)\phi - k_1az_{u1} + k_2bz_{u2} - k_3az_{u3} + k_4bz_{u4} = 0, \quad (3.8)$$

$$m_{w1}\ddot{z}_1 - c_1\dot{z}_s - c_1f\dot{\theta} - c_1a\dot{\phi} + (c_1 + c_{t1})\dot{z}_{u1} - k_1z_s - k_1f\theta - k_1a\phi + (k_1 + k_{t1})z_{u1} = k_{t1}z_{g1} + c_{t1}\dot{z}_{g1}, \quad (3.9)$$

$$m_{w2}\ddot{z}_2 - c_2\dot{z}_s - c_2f\dot{\theta} + c_2b\dot{\phi} + (c_2 + c_{t2})\dot{z}_{u2} - k_2z_s - k_2f\theta + k_2b\phi + (k_2 + k_{t2})z_{u2} = k_{t2}z_{g2} + c_{t2}\dot{z}_{g2}, \quad (3.10)$$

$$m_{w3}\ddot{z}_3 - c_3\dot{z}_s + c_3d\dot{\theta} - c_3a\dot{\phi} + (c_3 + c_{t3})\dot{z}_{u3} - k_3z_s + k_3d\theta - k_3a\phi + (k_3 + k_{t3})z_{u3} = k_{t3}z_{g3} + c_{t3}\dot{z}_{g3}, \quad (3.11)$$

$$m_{w4}\ddot{z}_4 - c_4\dot{z}_s + c_4d\dot{\theta} + c_4b\dot{\phi} + (c_4 + c_{t4})\dot{z}_{u4} - k_4z_s + k_4d\theta + k_4b\phi + (k_4 + k_{t4})z_{u4} = k_{t4}z_{g4} + c_{t4}\dot{z}_{g4}. \quad (3.12)$$

3.2. Seat suspension analytical model

In this paper, the three-dimensional vertical-pitch-lateral vibration of the vehicle body is taken as the excitation at the base of a seat suspension. At the same time, the MR dampers (MRD) are adopted in the limbs $\{-S_{i1}-P_{i2}-S_{i3}-\}$ $(i = 1, 2)$. Therefore, the seat suspension analytical model is built in the Fig. 4, where k_{12} and k_{13} denote the spring constant, c_{12} and c_{13} are the damping coefficients of the damper, F_i $(i = 12, 13)$ are the forces when the semi-active control is employed; x_r, θ_z, and Φ_z represent the vertical, pitch and roll output at the seat's center of mass; x_{02}, x_{03} are the vibration input of the limbs $\{-S_{i1}-P_{i2}-S_{i3}-\}$ $(i = 1, 2)$, and x_{12}, x_{13} are their vibration output; m_r is the occupant mass. The main parameters of seat suspension are given in Table 1.

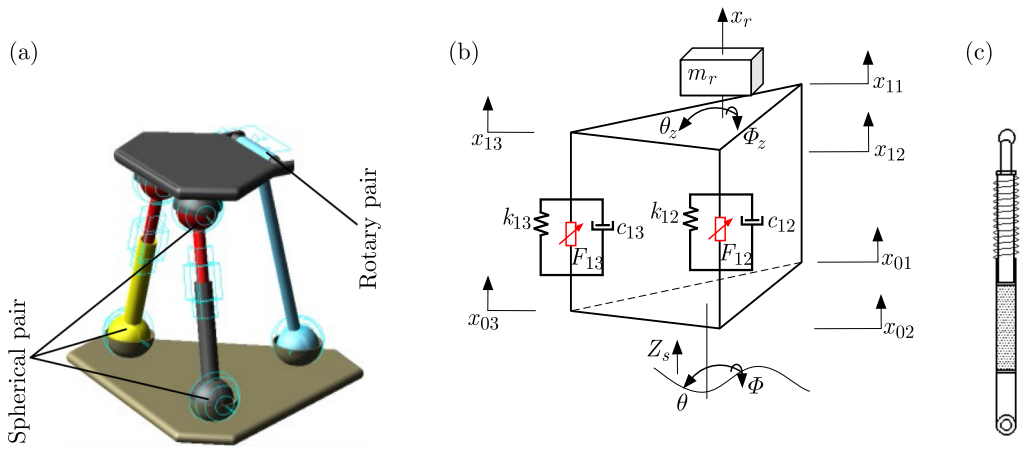

Fig. 4. 2SPS+SR parallel seat suspension: (a) seat suspension; (b) analytical model; (c) MRD.

Table 1. Main parameters of seat suspension.

Parameter description	Unit	Value
Occupant mass, m_r	Kg	75
Vehicle body mass, m_s	Kg	34000
Wheel axles mass	Kg	60
Tire stiffness	N/m	3.2e5
Vehicle suspension stiffness	N/m	4.95e4
Vehicle suspension damping	Ns/m	2250
Seat suspension stiffness	N/m	200
Seat suspension damping	Ns/m	0.6

According to Newton's law, the differential equation of the suspension seat is shown as follows:

$$m_r\ddot{x}_r = k_{12}(x_{02} - x_{12}) + c_{12}(\dot{x}_{02} - \dot{x}_{12}) + k_{13}(x_{03} - x_{13}) + c_{13}(\dot{x}_{03} - \dot{x}_{13}) - F_{12} - F_{13}, \tag{3.13}$$

$$I'_{yy}\ddot{\theta}_z = -[k_{12}(x_{02} - x_{12}) + c_{12}(\dot{x}_{02} - \dot{x}_{12}) - F_{12}]\frac{1}{2}r + [k_{13}(x_{03} - x_{13}) + c_{13}(\dot{x}_{03} - \dot{x}_{13}) - F_{13}]\frac{1}{2}r, \tag{3.14}$$

$$I'_{xx}\ddot{\phi}_z = [k_{12}(x_{02} - x_{12}) + c_{12}(\dot{x}_{02} - \dot{x}_{12}) - F_{12}]\frac{\sqrt{3}}{2}r + [k_{13}(x_{03} - x_{13}) + c_{13}(\dot{x}_{03} - \dot{x}_{13}) - F_{13}]\frac{\sqrt{3}}{2}r, \tag{3.15}$$

where I'_{yy} and I'_{xx} are the moment of inertia in the roll and pitch directions of the seat surface.

4. Fuzzy-PID control

A Fuzzy-PID controller is used to adjust the movement of the 2SPS+SR parallel suspension seat in real time, which is shown in Fig. 5. A commonly used fuzzy control system in this paper includes two-inputs and three-outputs, which takes the systematic error e and the error rate ec as input variables; e stands for the error between the actual acceleration a and the desired acceleration a_0 of the seat. And three-output variables are the automatic quantify factors of

proportional integral, and differential parameters k_p, k_i, and k_d. For the PID controller, its output u is defined as

$$u = k_p(a_0 - a) + k_i \int (a_0 - a)\,\mathrm{d}t + k_d \frac{\mathrm{d}}{\mathrm{d}t}(a_0 - a), \tag{4.1}$$

where

$$a_0 - a = e, \qquad \frac{\mathrm{d}}{\mathrm{d}t}(a_0 - a) = ec.$$

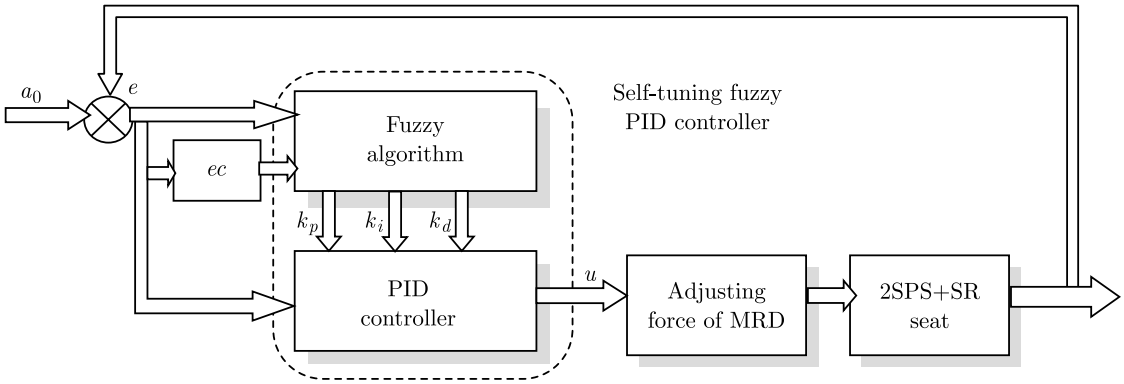

Fig. 5. Block diagram of self-tuning fuzzy-PID controller.

Tables 2–4 give the derived rule-bases. The fuzzy language is: NB – negative big, NM – negative medium, NS – negative small, ZE – zero, PS – positive small, PM – positive medium, PB – positive big. The physical domains of e and ec are $[-4, 4]$, and the domains of k_p, k_i, and k_d are $[-1, 1]$. The Gaussian membership function is used, and the control rule is the IF-Then. There are 49 rules to describe the relationship of the input and output numerical values in this article.

Table 2. Fuzzy control rule-base for k_d.

e	ec						
	NB	NM	NS	ZE	PS	PM	PB
NB	PS	PS	ZE	ZE	ZE	PM	PB
NM	NS	NS	NS	NS	ZE	NS	PM
NS	NB	NM	NM	NS	ZE	PS	PM
ZE	NB	NM	NM	NS	ZE	PS	PM
PS	NB	NM	NS	NS	ZE	PS	PS
PM	NM	NS	NS	NS	ZE	PS	PS
PB	PS	ZE	ZE	ZE	ZE	PB	PB

Table 3. Fuzzy control rule-base for k_i.

e	ec						
	NB	NM	NS	ZE	PS	PM	PB
NB	NB	NB	NB	NM	NM	ZE	ZE
NM	NB	NB	NM	NM	NS	ZE	ZE
NS	NM	NM	NS	NS	ZE	PS	PS
ZE	NM	NS	NS	ZE	PS	PM	PM
PS	NS	NS	ZE	PS	PS	PM	PM
PM	ZE	ZE	PS	PM	PM	PB	PB
PB	ZE	ZE	PS	PM	PM	PB	PB

Table 4. Fuzzy control rule-base for k_p.

e	ec						
	NB	NM	NS	ZE	PS	PM	PB
NB	PB	PB	PM	PM	PS	PS	ZE
NM	PB	PB	PM	PM	PS	ZE	ZE
NS	PM	PM	PM	PS	ZE	NS	NM
ZE	PM	PS	PS	ZE	NS	NM	NM
PS	PS	PS	ZE	NS	NS	NM	NM
PM	ZE	ZE	NS	NM	NM	NM	NB
PB	ZE	NS	NS	NM	NM	NB	NB

5. Simulation results and analysis

5.1. Vibration analysis on different road surfaces

When the vehicle is driven at a speed of 10 km/h, the simulation results for varying road surfaces and different controllers are shown in Figs. 6–8. At the same time, Table 5 shows root-mean-square (RMS) accelerations of the suspension. Figures 6–8 denote the fore-aft, lateral and vertical directions, respectively.

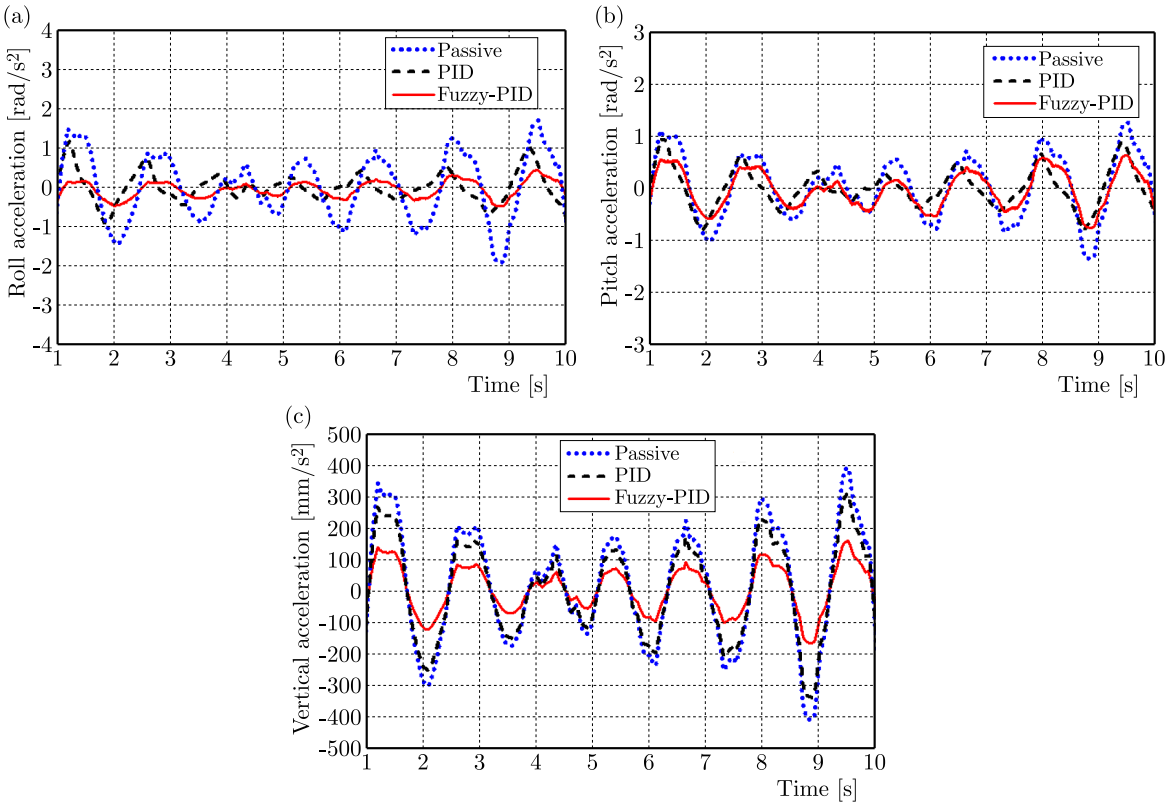

Fig. 6. Acceleration curves of seat under different control modes on E-level road: (a) roll; (b) pitch; (c) vertical.

A PID controller is developed in order to illustrate the improvement of the proposed fuzzy-PID. It can be seen from Figs. 6–8 that compared with the passive suspension seat, the PID and fuzzy-PID control suspension seat can effectively mitigate the vibrations.

In summary, the RMS accelerations of the 2SPS+SR seat using the fuzzy-PID controller in lateral, fore-aft and vertical directions are 0.149 rad/s^2, 0.195 rad/s^2, and 0.041 m/s^2 when the

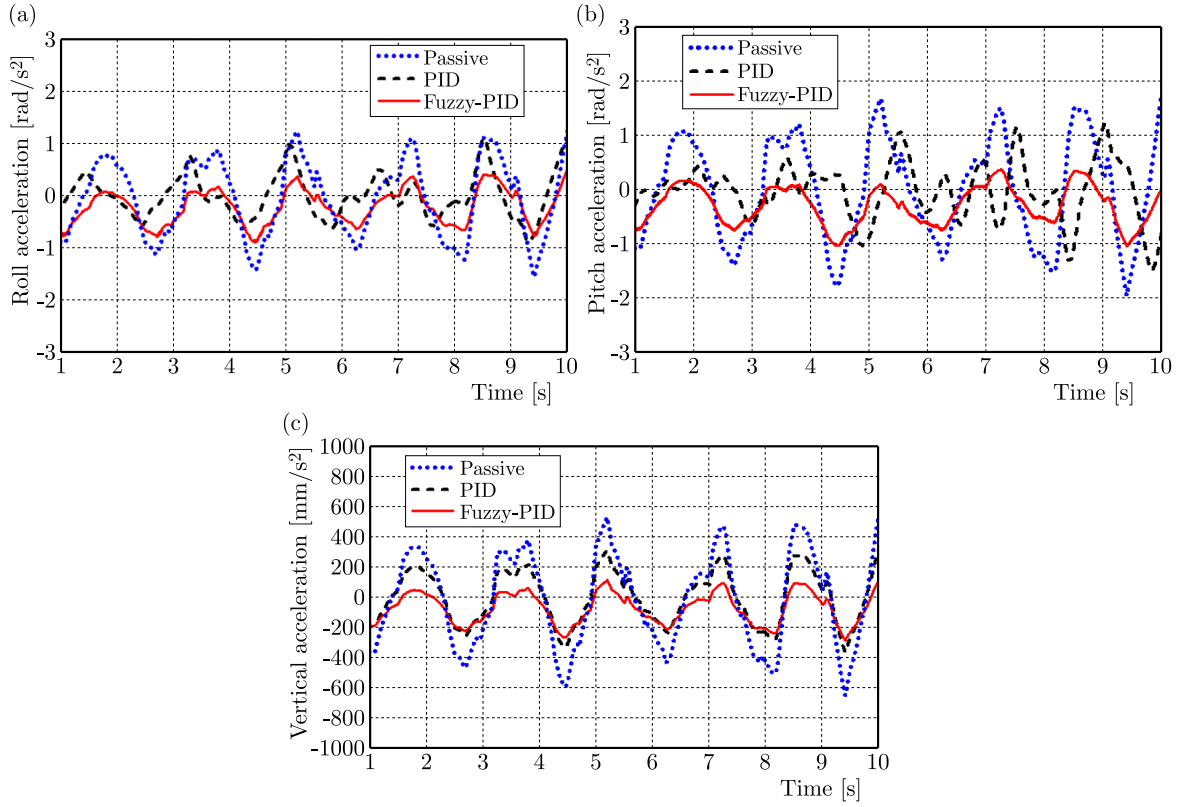

Fig. 7. Acceleration curves of seat under different control modes on F-level road: (a) roll; (b) pitch; (c) vertical.

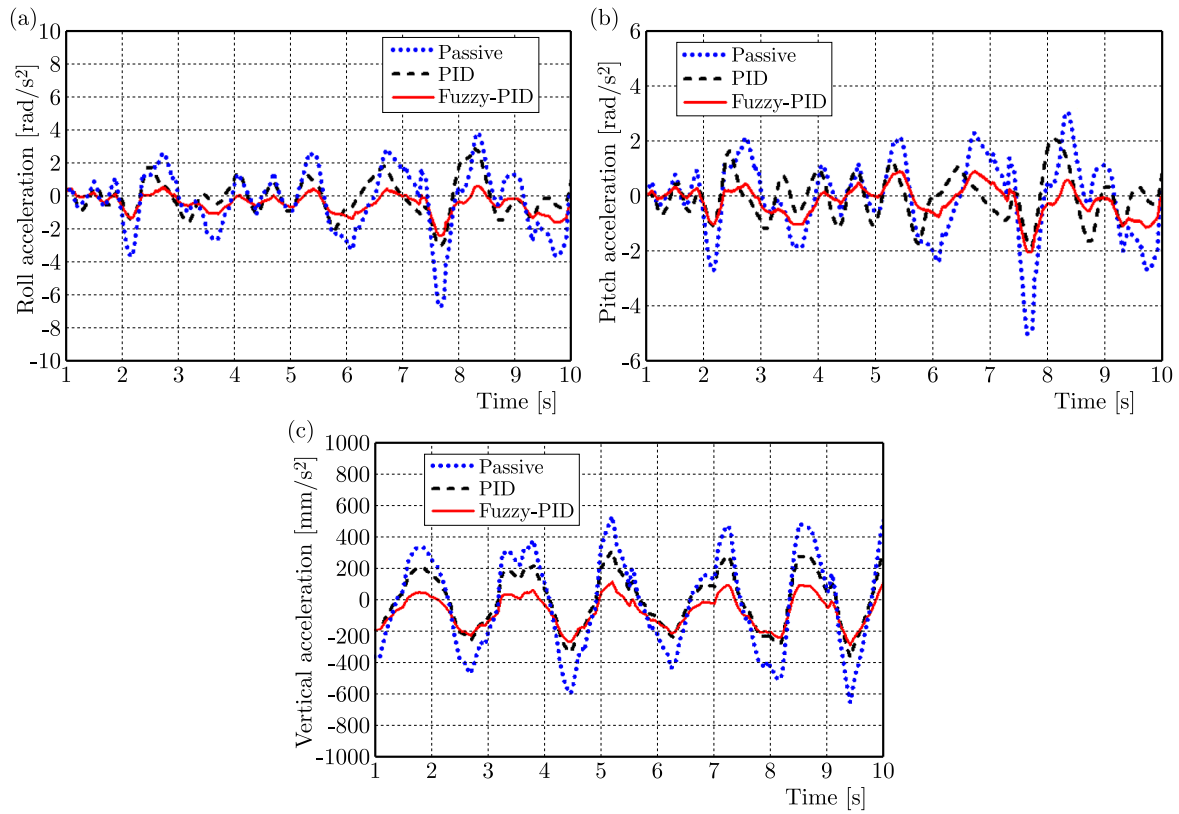

Fig. 8. Acceleration curves of seat under different control modes on G-level road: (a) roll; (b) pitch; (c) vertical.

vehicle is driven on E-class road. At the same time, the RMS accelerations using a simple PID controller are 0.255 rad/s^2, 0.236 rad/s^2, and 0.084 m/s^2, respectively. Similarly, for the F-class road, the acceleration responses using fuzzy-PID are 0.238 rad/s^2, 0.250 rad/s^2, and 0.072 m/s^2. And for the big excitation amplitude of the G-class road, the acceleration using the fuzzy-PID controller are 0.618 rad/s^2, 0.349 rad/s^2, and 0.163 m/s^2. Therefore, the fuzzy-PID provides better control effects than PID at this time.

Based on Table 5, it can be calculated that improvements of acceleration performance under different roads by the PID and fuzzy-PID controllers. The calculation results are shown in Fig. 9.

Table 5. Comparison of RMS accelerations for different roads and controllers.

Road	Modes	Lateral (a_{xw}) [rad/s^2]	Longitudinal (a_{yw}) [rad/s^2]	Vertical (a_{zw}) [m/s^2]
E	Passive	0.469	0.339	0.105
	PID	0.255	0.236	0.084
	Fuzzy-PID	0.149	0.195	0.041
F	Passive	0.763	0.446	0.145
	PID	0.262	0.373	0.083
	Fuzzy-PID	0.238	0.250	0.072
G	Passive	1.844	0.912	0.267
	PID	0.702	0.540	0.169
	Fuzzy-PID	0.618	0.349	0.163

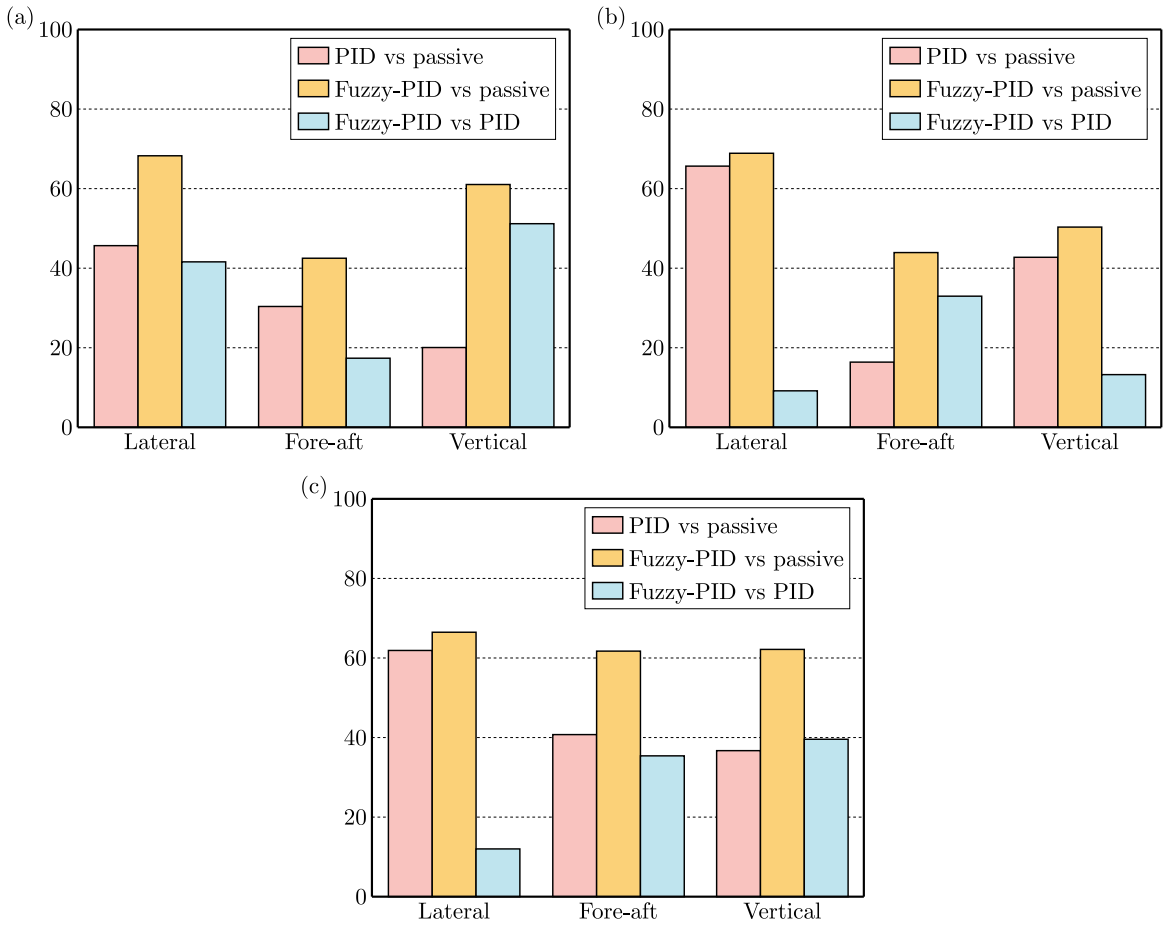

Fig. 9. RMS acceleration reduction – passive vs PID vs fuzzy-PID: (a) E-level road; (b) F-level road; (c) G-level road.

From Fig. 9, it could be known that the fuzzy-PID controller reduces the RMS accelerations by 68.23 %, 42.48 %, 60.95 % from those of a passive system in lateral, fore-aft and vertical directions under E-level road. The RMS accelerations of the PID system reduce 45.62 %, 30.38 %, and 20 % than those of the passive system. More importantly, the accelerations are successfully controlled by the proposed fuzzy-PID controller, which decrease 41.57 %, 17.3 %, and 51.19 % compared with those of the PID controller. Similarly, under F-class road, the fuzzy-PID controller reduces the RMS accelerations by 9.16 %, 32.98 %, 13.25 % from those of the PID controller in lateral, fore-aft and vertical directions. Under G-class road, the acceleration improvements can also be seen, the reductions of the fuzzy-PID system are 11.97 %, 35.37 %, and 39.52 % than those of PID controller. In sum, the fuzzy-PID could obviously reduce the acceleration amplitudes when compared with the PID one.

5.2. Ride comfort analysis of 2SPS+SR seat

The international standard ISO 2361-1997(E) is a general standard for vibration. Considering that the vehicle is subjected to vibration from three different directions, the total weighted acceleration RMS for the three axial directions is given as follows:

$$a_V = [1.4a_{xw}^2 + 1.4a_{yw}^2 + a_{zw}^2]^{1/2}, \tag{5.1}$$

where values of a_{xw}, a_{yw}, and a_{zw} from Table 5.

The weighted vibration level formula is obtained as

$$L_{av} = 20\lg(a_v/a_0), \qquad a_0 = 10^{-6}\,\mathrm{m/s^2}. \tag{5.2}$$

Table 6 shows the relationship between the weighted RMS value of acceleration, weighted vibration level, and human subjective feelings given by (ISO 2631-1, 1997) standard.

In order to further verify the damping effect of the 2SPS+SR suspension seat, the total weighted RMS of acceleration and the weighted vibration level are calculated based on the above Subsection 5.1 analysis results under different control modes. The computation results are shown in Tables 6–8.

Table 6. Comfort level under E-class road.

Modes	a_v [m/s^2]	L_{av} [dB]	Comfort level
Passive	0.159	104	Comfortable
PID	0.110	101	Comfortable
Fuzzy-PID	0.065	96	Comfortable

Table 7. Comfort level under F-class road.

Modes	a_v [m/s^2]	L_{av} [dB]	Comfort level
Passive	0.186	105	Comfortable
PID	0.126	102	Comfortable
Fuzzy-PID	0.101	100	Comfortable

Table 8. Comfort level under G-class road.

Modes	a_v [m/s^2]	L_{av} [dB]	Comfort level
Passive	0.409	112	Comfortable
PID	0.250	108	Comfortable
Fuzzy-PID	0.159	103	Comfortable

Through comparison of Tables 6–8 with international standards (ISO 2631-1, 1997), it could be known that the total weighted RMS of acceleration and the weighted vibration level using

a passive system are slightly larger than 0.315 m/s^2 and 110 dB, whose ride is "discomfortable". When the PID controlled suspension are installed in the seat, the ride is "not discomfort" when the vehicles driving under E- and F-class roads, but the L_{av} is equal to 108 dB and it is very close to the 110 dB on G-class roads. This phenomenon is caused owing to its fixed PID gains. When the 2SPS+SR seat controlled by the fuzzy-PID, the ride is 'not discomfort' when driving on E-, F-, G-class roads. As compared to the passive control and the PID control, the fuzzy-PID control leads to better vibration suppression.

6. Conclusions

In this paper, based on the single-open-chain theory, vertical-pitch-lateral movements are verified of the new type 2SPS+SR suspension seat. And the motion differential equations of the seven-DOF vehicle and three-DOF 2SPS+SR suspension seat are established, the proposed fuzzy-PID controller is designed for the semi-active suspension seat to obtain self-tuning of the gain parameters.

The simulation results prove that, the RMS accelerations of the 2SPS+SR seat using the fuzzy-PID controller in lateral, fore-aft and vertical directions are 0.149 rad/s^2, 0.195 rad/s^2, and 0.041 m/s^2 under the E-class road condition and the RMS accelerations under the F-class road are 0.238 rad/s^2, 0.250 rad/s^2, and 0.072 m/s^2, and the RMS accelerations under the G-class road are 0.618 rad/s^2, 0.349 rad/s^2, and 0.163 m/s^2, respectively. The fuzzy-PID controller can get better vibration-reducing effects than the PID system. The comfort levels are computed at the same time and a successful improvement could also be seen when the fuzzy-PID controller is adopted.

Acknowledgments

The authors would like to thank the Graduate Student Research Innovation Program of Shanxi Province (grant no. 2024KY644) for their support.

References

1. Abdul Zahra, A.K. & Abdalla, T.Y. (2020). Design of fuzzy super twisting sliding mode control scheme for unknown full vehicle active suspension systems using an artificial bee colony optimization algorithm. *Asian Journal of Control*, *23*(4), 1966–1981. https://doi.org/10.1002/asjc.2352
2. Deng, L., Sun, S., Christie, M., Ning, D.H., Jin, S., Du, H., Zhang, S. & Li, W. (2022). Investigation of a seat suspension installed with compact variable stiffness and damping rotary magnetorheological dampers. *Mechanical Systems and Signal Processing*, *171*, Article 108802. https://doi.org/10.1016/j.ymssp.2022.108802
3. Desai, R., Guha, A., & Seshu, P. (2021). Modelling and simulation of active and passive seat suspensions for vibration attenuation of vehicle occupants. *International Journal of Dynamics and Control*, *9*(4), 1423–1443. https://doi.org/10.1007/s40435-021-00788-2
4. International Organization for Standardization. (1977). *Mechanical vibration and shock – Evaluation of human exposure to whole-body vibration – Part 1: General requirements* (ISO Standard No. 2631-1:1997). https://www.iso.org/standard/7612.html
5. Jain, S., Saboo, S., Pruncu, C.I., & Unune, D.R. (2020). Performance investigation of integrated model of quarter car semi-active seat suspension with human model. *Applied Sciences*, *10*(9), Article 3185. https://doi.org/10.3390/app10093185
6. Jereczek, B., Maciejewski, I., Krzyzynski, T., & Krolikowski, T. (2023). Implementation of the SMC control strategy to an active horizontal seat suspension system. *Procedia Computer Science*, *225*, 3527–3535. https://doi.org/10.1016/j.procs.2023.10.348
7. Khan, L., Qamar, S., & Khan, U. (2016). Adaptive PID control scheme for full car suspension control. *Journal of the Chinese Institute of Engineers*, *39*(2), 169–185. https://doi.org/10.1080/02533839.2015.1091427

8. Maciejewski, I., Zlobinski, M., Krzyzynski, T., & Glowinski, S. (2020). Vibration control of an active horizontal seat suspension with a permanent magnet synchronous motor. *Journal of Sound and Vibration*, *488*, Article 115655. https://doi.org/10.1016/j.jsv.2020.115655

9. Ni, D.K., Van Liem, N., & Li, S.M. (2023). Performance analysis of the seat suspension using different models of the optimal negative-stiffness-structures. *Proceedings of the Institution of Mechanical Engineers, Part D: Journal of Automobile Engineering*, *237*(6), 1313–1326. https://doi.org/10.1177/09544070221091040

10. Sun, C., Liu, C., Zheng, X., Wu, J., Wang, Z.M., & Qiu, Y. (2023). An analytical model of seated human body exposed to combined fore-aft, lateral, and vertical vibration verified with experimental modal analysis. *Mechanical Systems and Signal Processing*, *200*, Article 110527. https://doi.org/10.1016/j.ymssp.2023.110527

11. Tan, V.V., Hung, T.M., & Sename, O. (2021). An investigation into the ride comfort of buses using an air suspension system. *International Journal of Heavy Vehicle Systems*, *28*(2), 184–205. https://doi.org/10.1504/IJHVS.2021.115595

12. Wu, W.G., Ma, L.Z., Yang, Q.Z., & Chen, X.X. (2011). 3-D vibration isolation of vehicle seat based on parallel mechanism (in Chinese). *Transactions of the Chinese Society of Agricultural Machinery*, *42*(6), 23–27.

13. Yan, B.J., Liu, Z.K., Zhang, W.J., & Liu, S.Z. (2022). Dynamic characteristics analysis of tubular stand-off layer sandwiched structure used in driving sprocket. *International Journal of Heavy Vehicle Systems*, *29*(2), 163–179. https://doi.org/10.1504/IJHVS.2022.125316

14. Yang, T.L. (2012). Theory and application of robot mechanism topology (in Chinese). Beijing: Science Press.

15. Zhang, J.H., Xu, Z.Y., Li, D.S., & Liu, H. (2015). Research on vibration damping device of vehicle seat based on 3-RPC parallel mechanism (in Chinese). *Mechanical Design*, *32*(2), 26–31.

16. Zhang, N. & Zhao, Q. (2017). Fuzzy sliding mode controller design for semi-active seat suspension with neuro-inverse dynamics approximation for MR damper. *Journal of Vibroengineering*, *19*(5), 3488–3511. https://doi.org/10.21595/jve.2017.17654

Manuscript received May 25, 2024; accepted for publication February 10, 2025; published online April 14, 2025.